MINIMAL INVASIVE BEAM PROFILE MONITORS FOR HIGH INTENSE HADRON BEAMS

Peter Forck
GSI Helmholtzzentrum für Schwerionenforschung, Darmstadt, Germany

Abstract

Beam profile determination at high intensity hadron accelerators implies the usage of non-destructive methods. The basic physics and recent technical realizations of important non-intercepting profile diagnostics are summarized. This contribution covers Ionization Profile Monitors, Beam Induced Fluorescence Monitors, transverse electron beam scanners, laser beam scanners used at H^- LINACs, Optical Transition Radiation screens and Synchrotron Radiation Monitors for relativistic beams.

PROFILE MEASUREMENT DEMANDS

Non-destructive transverse profile measurements are preferred not only for single-path diagnostics at different locations in a transfer line, but also to enable time resolved observations of a stored beam within a synchrotron. A more practical, however essential reason for minimal invasive diagnostics is the large beam power available at modern hadron accelerators, which excludes the usage of intercepting methods like scintillation screens, SEM-grids or wire scanners due to the risk of melting when irradiated by the total beam intensity.

Various methods for profile determination are realized to determine the properties of typical widths $\sigma = 0.1$ to 10 mm of not necessarily Gaussian shapes. The first class is based on atomic collisions between the beam ions and the residual gas: The direct detection of ionized residual gas ions or electrons with an Ionization Profile Monitor (IPM) and the detection of single photons from excited levels of the residual gas by Beam Induced Fluorescence (BIF). A second class uses the deflection of an intersecting electron beam by the space charge of the hadron beam for profile reconstruction. These methods can be applied for all hadron beams and the main matter of this article is the description of their basic physics and recent technical realizations. On the contrary, other methods call for dedicated beam conditions: For negative H^- beams the loosely bound electron can be detached with an optical photon as provided by a laser scanner. For relativistic hadron beams, Optical Transition Radiation (OTR) screens and Synchrotron Radiation Monitors (SRM) provides sufficient signal strength.

IONIZATION PROFILE MONITOR

In most synchrotrons and storage rings the transverse profile of the circulating beam is monitored via detecting the ionization products from the collision of hadrons with residual gas by an Ionization Profile Monitor. Inside the

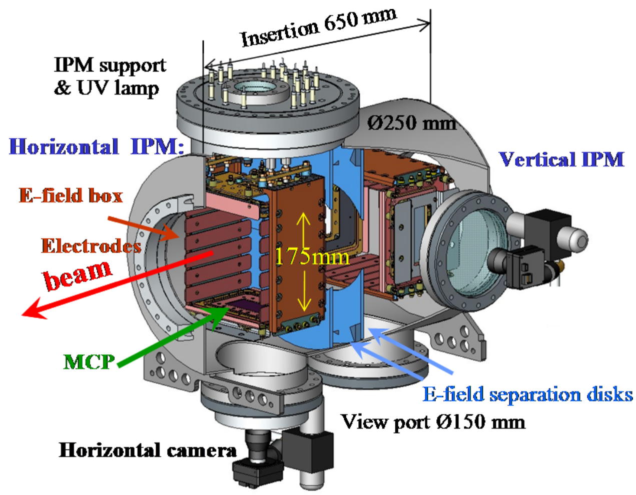

Figure 1: Schematic view of the IPM installation at GSI Storage Ring ESR and FZ-Jülich COSY [1].

vacuum tube a set of biased electrodes produces an electric field of typically 50 to 300 kV/m with a maximal voltage of 50 kV [2]. In this electric field the residual gas electrons or ions are accelerated towards a spatially resolving Micro-Channel Plate (MCP), as shown in Fig. 1. In order to receive an undistorted image of the beam density the residual gas ions have to be guided on straight trajectories toward the MCP detector. This requires an electrical field homogeneity of about 1 %, which is achieved by two main electrodes on top and bottom, and typically 5 to 10 side electrodes biased accordingly. To allow for a shorter insertion length the field quality can be improved with additional field forming electrodes biased with higher potential than the main electrodes, as calculated by Finite Element Codes [3]. Detailed calculations of the residual ion's trajectory in a realistic electric field were performed taking the space charge field of the beam into account [2, 4, 5].

Residual gas ions or electrons are detected and amplified with an MCP of typical size 100x50 mm^2. Depending on the expected count rate, which is determined by the beam current and the vacuum pressure, either a single MCP is installed with $\simeq 10^3$ electron-multiplication, or a double MCP assembly (Chevron configuration) with $\simeq 10^6$ multiplication is used. A single MCP offers a spatial resulution of about 20 μm and a double MCP of 50 μm.

The type of MCP readout is a compromise between the spatial and time resolution, two different readout technologies are commonly used:

Phosphor screen: The electrons create light spots on a phosphor screen behind the MCP, which are monitored by a CCD camera, as used for the setup in Fig. 1. An overall resolution of typically 100 μm is achieved. This method is preferred for high energy synchrotrons, delivering low emittance beams [6], and in cooler rings [1]. A typical time resolution is in the order of 1 to 10 ms, as given by the frame rate of the camera. To enable a μs time resolution, as required for a turn-by-turn readout, a multi-anode photomultiplier [6] has to be installed as an additional fast readout system. Alternatively, an avalanche photo-diode array or the recently available Silicon Photomultiplier (SiPM) were tested [7].

Wire array: An array of wires is mounted behind the MCP to collect the current of amplified electrons. The spatial resolution is limited by the distance of the anode wires having a pitch down to 0.25 mm [8]. But it is possible to get a time resolution of $\simeq$100 ns using sensitive broadband amplifiers [9] or charge-sensitive amplifiers [10].

After reaching a certain irradiation level the MCP-channels show a non-recoverable degradation of amplification caused by the amplified electrons at the exit side of the MCP. To perform a software correction of this local non-uniformity of MCP-amplification a test device must be foreseen. Opposite to the MCP an Electron Generator Plate can be mounted (EGP, an MCP biased to yield electron field emission) [2, 11]. Alternatively, the MCP can be homogeneously illuminated by a UV-lamp [12], as realized for the setup in Fig. 1.

IPMs detect either residual ions or electrons depending on the voltage polarity of the applied electric field. For low current beams residual ion detection is preferred: Due to the scattering kinematics a negligible momentum is transferred to the residual gas ions and they are accelerated towards the MCP on straight trajectories as determinated by the external electric field. For high beam intensities, the beam's space-charge field $\mathbf{E}_{SC}$ is comparable to the IPM electric field. To overcome the influence of $\mathbf{E}_{SC}$ an electron detection scheme is used, where the electrons are additionally guided by an external magnetic dipole field of typically $B = 100$ mT [2]. This value is chosen so that the cyclotron radius r_c along a field line is comparable to the resolution of the MCP. The cyclotron radius $r_c = m_e v_\perp / eB$ is determined by the initial electron velocity $v_\perp$ perpendicular to the B-field after the atomic collision. From model calculations using a simplified 'binary encounter approximation' it is estimated that 90 % of these electrons are emitted with kinetic energies below 50 eV, resulting in $r_c < 100$ μm [5]. A well-defined B-field of uniformity below 1 % is required along the full path of the residual gas electrons from the interaction point to the MCP (up to 100 mm) in order to yield an undistorted beam image [2, 5]. Different magnet designs were realized, using either electro-magnets [2, 6] or permanent magnets [9, 13]. The steering of the hadron beam caused by this dipole field, must be compensated by two additional dipoles with a reversed field. Due to the large aperture and the magnetic coupling between these dipoles an insertion length up to several meters is required [5, 2].

One important application is the observation of electron or stochastic cooling processes, e.g. [12, 14]. The transverse beam evolution during acceleration and storage as well as emittance variation during any beam manipulation is observed by IPMs, e.g. [15, 16]. For these processes significant changes of the transverse profile are slow compared to the revolution period, therefore a ms time resolution is sufficient furthermore a high spatial resolution by a phosphor screen anode is well suited for this application.

But also fast processes must be monitored on a turn-by-turn basis [17]. A prominent example is the control of the injection matching into a synchrotron, examples are presented in [2, 6, 9, 10]. Since usually the vacuum pressure in a synchrotron is as low as 10^{-11} mbar, a controlled pressure bump might be necessary to increase the residual gas ionization events. For sufficient statistics within one bunch passage at least 100 ionization events have to be detected during a time of down to 100 ns. To overcome the regular count rate limit of MCPs a time selected HV-switching is required, see e.g. [13].

In contrary to synchrotrons the residual gas density in transfer lines is some orders of magnitude larger. In particular, at a LINAC facility the ionization rate can be large enough that no MCP as the first stage amplifier is required. A direct registration of the residual gas ions on a wire array followed by sensitive current-to-voltage amplifiers [18] is possible. This reduces the mechanical efforts for an IPM significantly.

BEAM INDUCED FLUORESCENCE

Instead of detecting the ionic fragments as for an IPM, a Beam Induced Fluorescence Monitor images the fluorescence photons, as schematically depicted in Fig. 2. Due to the electronic stopping power the residual gas is ionized and left in an excited state with a certain probability. Only those photons emitted towards the camera are detected resulting in a typical value of solid angle $\Omega \simeq 10^{-4}$. The spatial resolution is adapted to the beam parameters over a wide range by choosing an appropriate optical magnification ratio. The boundary condition is the focal depth, which has to cover the entire beam diameter.

In order to detect single photons an image intensified camera has to be used. One technical principle is the MCP-based image intensifier which consists of a photo cathode, a MCP and a phosphor screen, which is observed by a camera. Image intensifiers are either available with a single MCP or a double MCP stack for single photon detection. Alternatively, a segmented photo-multiplier was used [19, 20]. As a third possibility a modern electron-multiplying CCD camera (emCCD) was considered [21]: The amplification of the photo-electrons is done by a chain of avalanche diodes between the CCD matrix and the ADC. This technique offers a higher spatial resolution but suffers from larger thermal noise in comparison to an image intensifier.

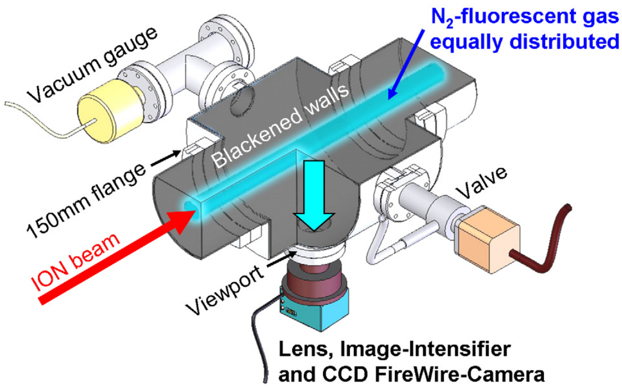

Figure 2: Scheme of a Beam Induced Florescence monitor for horizontal profile determination [24].

The BIF method is well suited for profile measurements at cw-LINAC [22, 23], pulsed LINAC [24, 25] an cyclotron facilities. Such monitors are installed e.g. at the pulsed GSI ion LINAC at several locations and used for standard operation [26]. Due to the single photon mode, beam profile can be determined within one single macro-pulse of 0.1 ms length. A different modern layout allowing for long integration time is described in [27].

At several laboratories [20, 23, 28] the method was applied for protons and light ions of typically 100 keV in the LEBT section behind the ion source. Due to the Doppler-shift spectra one can distinguish between fluorescence originating from the residual gas (nearly at rest) and light emitted by the beam particles after recombination with electrons of the residual gas.

Detailed investigations were performed on monitoring of stored beams inside a synchrotron as well. At CERN the photon yield and the wavelength spectrum were measured for proton beams on a wide scale of energies from 50 MeV up to 450 GeV [19, 29] for N_2 and *Xe* gas. It has been shown that the relative photon yield as a function of ion energy scales according to the Bethe-Bloch equation. This scaling was confirmed for different ion beams in an energy range of 60 to 750 MeV/u [25]. At BNL-RHIC the method was successfully applied for protons and gold ions using a hydrogen gas jet target [30].

The driving mechanism for BIF is an effective conversion of the ion's energy loss to a photon in the optical wavelength range via an excited state of the residual gas. The fluorescence yield and the wavelength spectra of rare gases and N_2 were extensively investigated using an imaging spectrograph [31]. With the exception of *He*, all transitions originate from ionized rare gases or N_2^+ and it was proven that the transverse profiles coincide for all spectral lines. For the case of *He* spectral line shows a significant broadening of the beam image. Therefore, *He* is excluded as a working gas. For H_2 as the working gas, the optical spectrum is composed of the Balmer Series of H-atoms [28, 30] and allows for reliable profile measurements.

The relative fluorescence yields of different working gases under an ion impact of 5.2 MeV/u are compared in

Table 1: Florescence yield Y of rare gases relative to N_2 for 10^{-3} mbar pressure and normalized to the electron density $Y_{dE/dx} = Y/Z$ for S^{6+} ions at 5.2 MeV/u [31].

Gas	*Xe*	*Kr*	*Ar*	*He*	N_2
Y [%]	86	63	38	4	100
$Y_{dE/dx}$ [%]	22	25	30	26	100

Table 1. To include the energy loss dE/dx of the beam ions in the gas, the fluorescence yield is normalized to the electron density represented by the atomic number of the working gas Z or $2Z$ for N_2. It has to be emphasized that the fluorescence yield per unit of energy loss of all rare gases is nearly similar but is a factor of $\simeq$4 lower compared to N_2 [31]. In the case of *Xe* working gas comparable results were obtained for proton impact in the energy range from 1.4 to 25 GeV [19]. Further measurements at RHIC with 100 GeV/u proton and gold beams [30] shows that the fluorescence yield of H_2 as working gas is even a factor of 5 lower compared to N_2. Due to the concentration in the blue wavelength range N_2 offers the best performance and is well suited from a point-of-view of vacuum issues. Furthermore, for N_2 it was demonstrated that the signal strength is proportional to the vacuum pressure in the range between 10^{-6} and 10^{-1} mbar and the recorded profile width is independent of the pressure [25].

The lifetimes of the N_2 excited states were measured to be $\tau = 58.0(3)$ ns, which coincide for 25 GeV [19, 29] and 100 keV [32] proton impact. The lifetime for *Xe* is $\tau = 6.0(1)$ ns [19]. For high intensity hadron beams with sub-mm width the residual gas ions might be accelerated significantly by the beam's space charge (as discussed for the IPM) and therefore the short lifetimes of *Xe* is an advantage to prevent for artificial image deformations.

Background contributions might spoil the image quality due to the sensitivity of the photo-cathode to other types of radiation. Namely to high energetic gamma rays and neutrons which penetrate the image intensifier housing, see e.g.[21, 25]. Because the production rate of the radiation increases strongly with the hadron's energy, an effective shielding of the image intensifier and camera is required. For this arrangement the fluorescence photons have to be transfered to the sensor either by a telescope arrangement or by a fiber based image guide [21, 27, 33].

ELECTRON BEAM SCANNER

The transverse profile is reconstructed from the deflection of electrons crossing the hadron beam and being influenced by the beam's space charge , as schematically shown in Fig. 3. Assuming the electron beam has a much lower diameter than the hadron beam and the scan duration is much shorter than the ion bunch passage, the space charge field can be treated as constant. The deflection angle is maximal at the beam edge and decreases during the scan towards the beam center; no deflection occurs when passing the center.

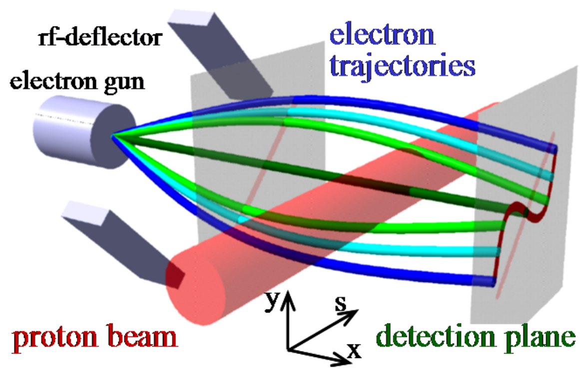

Figure 3: Schematics of an electron scanner for the vertical profile.

The electron trace in the detector plane is recorded. The diagonal deflection makes sure that the profile information is extracted from the derivative of this trace with respect to the beam direction. This method was considered for high energy synchrotrons [34, 35] and recently commissioned at SNS [36]. For low energetic beams the functionality was proven as well [37]. Using a scanning ion beam instead of electrons, the method was analyzed and tested at CERN [38]. The corresponding mathematical formalism for profile reconstruction is given in Refs. [35, 37, 38].

The setup at the SNS-Ring [36] consists of an electron gun providing electrons of maximal 75 keV and up to 5 mA current for 1 μs pulses at 5 Hz repetition rate. The beam passes an electric deflector for a diagonal sweep of 20 ns duration and two quadrupoles to enlarge the spatial range and parallelize the beam during scanning. After crossing the hadron beam, where the deflection occurs the electrons are visualized by a phosphor screen and recorded with a camera. To achieve a reasonable deflection, the electron beam energy has to be matched to the hadron beam current. The advantage is the possibility of sliced profile measurements with high time resolution as given by the short sweep duration of only 20 ns.

FURTHER TYPES OF MONITORS

Laser Scanner for H^- beams

Many high intensity LINACs accelerate H^-. The H^- electron binding energy is only 0.75 eV (corresponding to a wavelength of $\lambda = 1650$ nm) and it has a large cross section for photo-detachment of $4 \cdot 10^{-17}$ cm^2 at its maximum of 1.5 eV ($\lambda = 830$ nm). For profile measurements a focused laser beam is scanned through the H^- beam and the detached electrons or the neutral H^0 are detected. Alternatively, the decrease of the H^- current is measured.

This technology is applied at the SNS-LINAC for beam energies from 0.2 to 1 GeV [39]. One Q-switched Nd:YAG laser delivers 7 ns long pulses at $\lambda = 1060$ nm with an pulse energy of 50-200 mJ at 30 Hz repetition rate. The laser is located in a separated cabin and the laser beam is transported via stabilized mirrors over up to 250 m to one of 9 profile measurement locations. The laser beam is focused down to some 10 μm and scanned through the H^- beam to liberate electrons at the percent level of the passing H^-ions. These electrons are separated by a magnetic dipole field of $\simeq$20 mT towards a Faraday-Cup. Due to the short laser pulses a possible profile variation during the macro pulse can be observed. A compact design with a locally installed laser is presented in [40, 41]. Moreover, this method was applied at low energetic H^- just behind the ion source [42].

Optical Transition Radiation Monitor

The transit of charged particles between two media of different dielectric constants causes optical transition radiation (OTR) as emitted within a cone having its maximum at $1/\gamma$ and an intensity scaling at that angle as $I \propto \gamma^2$, with γ being the Lorentz-factor. Due to this scaling OTR monitors are well suited for electron beam profiling, but are also used more than 20 years for protons [43] with energies above 10 GeV. A 2-dim beam image is visible on the foil and is recorded by an image intensified camera. Because OTR is a pure surface phenomenon a thin foil down to μm thickness is sufficient. This leads to less heating by the beam's energy loss and significantly reduced particle straggling as compared to SEM-Grids or viewing screens. OTR monitors are usually installed in transfer lines and in front of production targets irradiated by high beam power, e.g. [44, 45]. They have a high radiation tolerance as proven by an irradiation of $6 \cdot 10^{19}$ protons at 120 GeV resulting in a decrease of light emission, but constant profile reading [44]. A further application is the installation within a high energy synchrotron, where the thin foil enables a turn-by-turn observation to determine the beam properties at injection [46, 47] offering higher spatial resolution and statistical accuracy compared to the usage of an IPM.

Synchrotron Radiation Monitor

Charged particles following a curved trajectory emits synchrotron radiation with an angular distribution and wavelength spectrum strongly depending on the Lorentz-factor γ, see e.g. [48]. Only for high relativistic protons of energies above typically 200 GeV the emission of optical photons is sufficiently intense for profile determination. The first monitor of this kind was realized at CERN-SPS for beam energies above 350 GeV [49] detecting the radiation emitted at a regular dipole. At FNAL-Tevatron [50, 51], DESY-HERA [52] and CERN-LHC [53] monitors observing the light from dipoles are realized as well. In order to detect sufficient optical photons over the whole proton acceleration range, the radiation from the dipole fringe field is observed or a dedicated undulator is installed. The resolution of about 100 μm is limited by diffraction within the optical path. A 2-dim online profile observation with a time resolution of typical 20 ms is feasable [53].

SUMMARY

IPMs are in operation at most hadron accelerators and are used for profile determination with a time resolution down to the μs scale and data recording during the full acceleration cycle. With an IPM all ionic fragments from the residual gas are collected. But there are some technical challenges to be solved due to the complex vacuum installation and the required magnets for electron guidance. For a BIF monitor the hardware is much simpler allowing for a compact installation. But due to the finite solid angle of $\Omega < 10^{-4}$, the signal is about 5 to 6 orders of magnitude lower as for an IPM equipped with an MCP. The time resolution for BIF is limited to the 100 μs range in a single shot mode. By changing the residual gas density the count rate for BIF and IPM is adjusted. With an electron scanner the profile can even be recorded within one bunch, but it has a low repetition rate. The laser scanner of H^- is now routinely operated, but several seconds are required to record a full profile. OTR screens are used for relativistic beams to deliver a 2-dim image, in particular they are used in front of a production target. A SRM is a very useful device at ultra-relativistic synchrotrons to deliver a profile within a time resolution of typically 20 ms. The applicability of several methods at the FNAL facility is summarized in [54, 55].

ACKNOWLEDGMENT

The valuable discussion with many colleagues is gratefully acknowledged. In particular I thank F. Becker (GSI), W. Blokland (ONL), C. Gabor (RAL), T. Giacomini (GSI), G. Kube (DESY), T. Lefevre (CERN), Y. Liu (ONL), J. Marroncle (CEA), J. Pogge (ONL), K. Satou (J-PARC), B. Walasek-Höhne (GSI) and J. Zagel (FNAL).

REFERENCES

[1] C. Böhme et al., *DIPAC'09*, p. 191 (2009).
[2] K. Satou et al., *EPAC'08*, p.1275 (2008) and K. Satou et al., *Porc. EPAC'06*, p. 1163 (2006).
[3] D. Liakin et al., *DIPAC'05*, p. 150 (2005).
[4] R.E. Williamson et al., *EPAC'08*, p.1317 (2008).
[5] V. Skachkov et al., *RuPAC'06*, p. 241 (2006) and D. Liakin et al., *DIPAC'05*, p. 154 (2005).
[6] G. Ferioli et al., *DIPAC'03*, p. 116 (2003) and C. Fischer et al., *BIW'04*, p. 133 (2004).
[7] D. Liakin et al., *DIPAC'07*, p. 90 (2007).
[8] A. Jansson et al., *PAC'05*, p. 2227 (2005).
[9] R. Connolly et al., *BIW'10* (2010) and R. Connolly et al., *PAC'01*, p. 1297 (2001).
[10] A. Jansson et al.,*EPAC'06*, p. 2777 (2006) and A. Jansson et al., *PAC'07*, p. 3883 (2007).
[11] H. Refsum et al., *DIPAC'05*, p. 160 (2005).
[12] T. Giacomini et al., *BIW'04,* p. 286 (2004) and T. Giacomini et al., *DIPAC'05*, p. 150 (2005).
[13] J.R. Zagel et al., *PAC'01*, p. 1303 (2001) and J.R. Zagel et al., *PAC'99*, p. 2164 (1999).
[14] C. Bal et al., *DIPAC'07*, p. 120 (2007).
[15] R. Connolly, R. Michnoff, S. Tepikian, *PAC'05*, p. 230 (2005).
[16] G. Franchetti et al., subm. to *Phys. Rev. Acc. Beams*(2010).
[17] J. Zagel et al., *BIW'10* (2010).
[18] J. Marroncle et al. *DIPAC'09*, p. 375 (2009).
[19] M.A. Plum et al., *Nucl. Instrum. Meth* **A 492**, p. 42 (2002).
[20] C. Böhme et al., *BIW'10* (2010).
[21] F. Becker et al., *BIW'08*, p. 236 (2008).
[22] D.P. Sandoval et al., *BIW'93*, p. 273 (1993).
[23] D.D. Chamberlin et al., Proc. PAC'81, p. 2347 (1981).
[24] P. Forck, A. Bank, *EPAC'02*, p. 1885 (2002) and A. Bank, P. Forck, *DIPAC'03*, p. 137 (2003).
[25] F. Becker et al., *DIPAC'07*, p. 33 (2007).
[26] R. Haseitl et al., *DIPAC'09*, p. 134 (2009) and C. Andre et al., *GSI Scientific Report 2008*, p. 124 (2008).
[27] J.M. Carmona et al., *DIPAC'09*, p.173 (2009).
[28] P. Ausset et al., *EPAC'02*, p. 1840 (2002).
[29] A. Variola, R. Jung, G. Ferioli, *Phys. Rev. Acc. Beams* **10**, 122801 (2007), G. Burtin et al., *EPAC'00*, p. 256 (2000).
[30] T. Tsang et al., *PAC'09*, p. 1 (2009) and T. Tsang et al., *Rev. of Sci. Instrum.* **79**, 105103 (2008).
[31] F. Becker et al., *DIPAC'09*, p. 161 (2009) and F. Becker et al., *BIW'10* (2010).
[32] R.H. Hughes et al., *Phys. Rev.* **123**, 2084 (1961), L.W. Dotchin et al., *J. Chem. Phys.* **59**, 3960 (1973).
[33] F. Senee et al., *DIPAC'09*, p. 197 (2009).
[34] A. Aleksandrov et al., *PAC'05*, p. 2586 (2005).
[35] E. Tsyganov et al.,*PAC'93*, p.2489 (1993).
[36] W. Blokland et al., *DIPAC'09*, p. 155 (2009).
[37] P.K. Roy et al., *Rev. of Sci. Instrum.* **76**, 023301 (2005).
[38] J. Bosser et al., *Nucl. Instrum. Meth* **A 484**, p. 1 (2002).
[39] Y. Liu et al., *Nucl. Instrum. Meth* **A 612**, p. 241 (2010), Y. Liu et al., *EPAC'08*, p. 1197 (2008) and R. Connolly et al., *LINAC'02*, p. 21 (2002).
[40] R. Connolly et al., *BIW'10*, (2010) and R. Connolly et al., *LINAC'08*, p. 615 (2008).
[41] J. Pogge et al., *BIW'08*, p. 143 (2008).
[42] D.A. Lee et al., *DIPAC'09*, p. 393 (2009) and C. Gabor et al., *EPAC'06*, p. 1037 (2006).
[43] J. Bosser et al., *Nucl. Instrum. Meth.* **A 238**, p. 45 (1985).
[44] V.E. Scarpine, G.R. Tassotto, A.H. Lumpkin, *PAC'07*, p. 2639 (2007) and V.E. Scarpine et al., *PAC'05*, p. 2381 (2005).
[45] A. Toyoda et al., *DIPAC'09*, p. 372 (2009).
[46] C. Bovet et al., *DIPAC'99*, p. 90 (1999).
[47] V.E. Scarpine, A.H. Lumpkin, G.R. Tassotto, *BIW'06*, p. 473, (2006).
[48] G. Kube, *DIPAC'07*, p. 6 (2007).
[49] R. Bossart et al., *Nucl. Instrum. Meth.* **164**, p. 375 (1979), J. Bosser et al., *PAC'83*, p.2164 (1983).
[50] A.A. Hahn, P. Hurh, *PAC'91*, p. 1177 (1991).
[51] R. Thurman-Keup, *BIW'06*, p. 364 (2006) and H.W.K. Cheung, A. Hahn, A. Xiao, *PAC'03*, p. 2488 (2003).
[52] G. Kube et al., *BIW'06*, p. 374, (2006).
[53] T. Lefevre et al., *IPAC'10* (2010), A.S. Fisher, A. Goldblatt, T. Lefevre, *DIPAC'09*, p. 164 (2009) and R. Maccaferri et al., *EPAC'04*, p. 1630 (2004).
[54] M. Wendt et al., *HB'08*, Nashville, p. 440 (2008).
[55] J. Zagel et al., *BIW'08,* p. 393 (2008).